



OPEN ACCESS

EDITED BY

Jie Han,
University of Kansas, United States

REVIEWED BY

Rui Pang,
Dalian University of Technology, China
Fayun Liang,
Tongji University, China

*CORRESPONDENCE

Xiaoxuan Yu,
✉ yuxiaoxuan@tju.edu.cn

RECEIVED 21 February 2024

ACCEPTED 14 March 2024

PUBLISHED 25 March 2024

CITATION

Zhou H, Ma F, Yu X and Zheng G (2024), Fragility assessment for the rainfall-induced embankments on silty soils. *Front. Built Environ.* 10:1389576. doi: 10.3389/fbuilt.2024.1389576

COPYRIGHT

© 2024 Zhou, Ma, Yu and Zheng. This is an open-access article distributed under the terms of the [Creative Commons Attribution License \(CC BY\)](https://creativecommons.org/licenses/by/4.0/). The use, distribution or reproduction in other forums is permitted, provided the original author(s) and the copyright owner(s) are credited and that the original publication in this journal is cited, in accordance with accepted academic practice. No use, distribution or reproduction is permitted which does not comply with these terms.

Fragility assessment for the rainfall-induced embankments on silty soils

Haizuo Zhou^{1,2,3}, Fujian Ma^{1,2}, Xiaoxuan Yu^{1,2,3*} and Gang Zheng^{1,2,3}

¹School of Civil Engineering, Tianjin University, Tianjin, China, ²Key Laboratory of Coast Civil Structure Safety, Tianjin University, Ministry of Education, Tianjin, China, ³State Key Laboratory of Hydraulic Engineering Simulation and Safety, Tianjin University, Tianjin, China

The fragility curve expresses the probability that an asset exceeds some serviceability state for a given level of environmental perturbation or other loadings. It is an important component in the quantitative risk analysis and resilience evaluation of infrastructure exposed to natural hazards. Incidences of over-settlement of embankments are increasingly reported due to more intense and longer-duration rainfall events. This paper develops fragility curves for the rainfall-induced embankment settlement. For this purpose, an embankment incorporating enhanced seepage and displacement analysis within unsaturated soil conditions is modelled based on a reported case history. A Monte Carlo simulation is used for rainfall infiltration and embankment deformation analysis under various rainfall scenarios. Probability values are obtained to achieve three levels of damage states in terms of road embankment settlement. The parametric analysis produces the exceedance probability curves for various rainfall intensities, saturated permeabilities and embankment slope angles. This work offers an efficient tool for assessing fragility to rainfall-induced excessive settlement of embankments.

KEYWORDS

embankments, rainfall, probabilistic analysis, settlement, fragility curves

1 Introduction

Embankment structures have been increasingly reported to have experienced various levels of deformation during rainfall events, such as the 2014 Bosnia and Herzegovina rainfall and the 2012 Southern Europe rainfall (Winter et al., 2020; Martinović et al., 2018). These occurrences present significant challenges to transportation infrastructure, disrupting the seamless operation of roads, railways, and other essential components of the transport network (Wang et al., 2022). During the 2013–2014 heavy rainfalls in the United Kingdom, extensive damage to rail lines across the southwest was observed (Thorne, 2014), resulting in the disruption of access along these routes.

Historic events have demonstrated that rainfall may induce embankment damage including cracking, excessive settlement, and lateral spreading (Reeves et al., 2019; Winter et al., 2020). The damage mechanism of excessive settlement results from the reduction of near surface soil suctions due to infiltrating water, along with the downward movement of the wetting front (Martinović et al., 2018; Chen et al., 2021). Besides, changes in climate and the environmental conditions surrounding the slopes are commonly insufficiently considered in design. Therefore, it is of paramount importance to consider the environmental, weather and climate change effects on embankment performance (Reeves et al., 2019; Achillopoulou et al., 2020).

TABLE 1 Material property values used for numerical analysis.

Material	γ_t (kN/m ³)	c (kPa)	φ (°)	ν	E_s (MPa)	k_s (m/s)	S_r (%)	ψ (kPa)	T (m)
Embankment	20	54	36	0.3	60	5.77×10^{-6}	44.0	46.26	7.53
loess-like silty clay	19	35.2	20.4	0.34	16.35	5.77×10^{-6}	44.0–55.2	34.64–46.26	11
silty soil	18	8.53	18.7	0.3	13.30	1.27×10^{-6}	55.2–66.4	15.74–34.64	7
silty clay	20	52	13.2	0.36	15.02	1.47×10^{-6}	66.4–100	0–15.74	12

Note: γ_t = unit weight; c = cohesion; φ = angle of internal friction; ν = Poisson's ratio; E_s = compression modulus; k_s = saturated permeability; S_r = saturation; ψ = matric suction; T = soil layer thickness.

The fragility curve acts as an efficient tool that can be implemented in the risk and resilience analysis (Chen et al., 2023; Xu et al., 2023; Lu et al., 2024). Fragility curves represent the probability of the studied objective exceeding a specific damage state (DS). In road embankment seismic analysis, fragility curves have been developed for embankments on soft and liquefiable soils (Argyroudis and Kaynia, 2015; Zhou et al., 2023). Compared with the seismic fragility analysis of embankments, the assessment of embankments under the rainfall within the framework of fragility curves is limited (Argyroudis et al., 2019). Considering the increasing rainfall-induced embankment damage, assessment of the risk resistance of transportation infrastructure becomes imperative. Enhancing the resilience of embankments against rainfall hazards is vital for ensuring uninterrupted mobility and sustaining socio-economic development.

This study aims to develop a set of fragility curves to assess the fragility of embankments to rainfall-induced settlement. An embankment model is constructed using the finite difference method FLAC 3D (Itasca Consulting Group, 2017). The model accounts for various parameters, including rainfall intensities, slope angles, and saturated permeability levels, to quantify the potential risk associated with rainfall-induced settlement. A detailed analysis of the relevant curve characteristics is conducted to gain insights into the interrelationships among these factors and the fragility of embankments. The outcomes of this study provide an efficient and reliable tool for assessing the fragility of embankments to excessive settlement triggered by rainfall, thereby contributing to informed decision-making in the design, construction, and maintenance of road infrastructure.

2 Method

2.1 Numerical modelling

A finite difference method FLAC 3D (Itasca Consulting Group, 2017; Zheng et al., 2024a) is adopted to simulate the embankment in this study. A railroad embankment located in Qingdao, Shandong province, China, was reported by Chen et al. (2014) to investigate the embankment settlement in site for an unsaturated soil. Embankments with a height of 7.53 m, a slope of 1.5 H : 1 V and a 6.25 m wide crest are constructed on the soft soil layers. One-half of the embankments are modelled, and symmetrical boundary conditions are applied along the lateral boundaries, while both the horizontal and vertical displacements are fixed along the bottom boundary. The lateral boundaries of the model are simulated with rollers, while pins provide support to the

bottom. The numerical model parameters are chosen to be the same as Chen et al. (2014), as shown in Table 1. The behavior of the embankment and soft soils is simulated using a linearly elastic-perfectly plastic Mohr-Coulomb constitutive model (Huang and Han, 2009; Zheng et al., 2019; Zhou et al., 2024). A staged construction is applied to represent the embankment load, and a 0.5 m high filling is constructed in each stage. With regard to hydraulic boundary conditions, a zero-pore pressure boundary condition is applied at the top of the soft clay layers and hence it is permeable (Zheng et al., 2024b). At the bottom of the mesh, an impervious boundary condition is employed. An impermeable boundary condition is applied to the left and right-hand side vertical boundaries because they are far from the loaded area. The excess pore pressures developed near these vertical boundaries are nearly zero throughout the analysis.

2.2 Fragility analysis

Probabilistic techniques are well-suited for analyzing rainfall-induced damages as both the load (i.e., disturbing force induced by rainfall) and the resistance (depends on soil suction) vary over time due to climatic factors (Babu and Murthy, 2005; Xue and Gavin, 2007; Gavin and Xue, 2009; Reale et al., 2016b). A framework is presented for interpreting serviceability state than traditional deterministic design which assumes fixed point values (Reale et al., 2015). If the probability distributions of both the limiting tolerable displacement and the calculated displacement S are known, then a fully reliability-based serviceability evaluation can be conducted. The reliability evaluation would be analogous to that of the serviceability limit evaluation. The performance function $g(X)$ for the serviceability limit can be written as the difference between an embankment capacity C and its demand D , as shown in Eq. 1:

$$g(X) = (C - D) \begin{cases} > 0, \text{ safe state} \\ = 0, \text{ limit state} \\ < 0, \text{ failure state} \end{cases} \quad (1)$$

where $g(X) > 0$ defines a satisfactory performance region and $g(X) < 0$ defines an unsatisfactory performance region. The main steps to derive fragility curves based on numerical modelling are the following.

1. Derive a model including the studied embankment and the imposed hazard effects (i.e., rainfall), and perform numerical analysis for increased hazard intensities. An infiltration analysis was carried out to analyze the influx of water into

the embankment with time. The progression of the wetting front over time is tracked by monitoring the time taken for each element to reach its residual suction.

2. Define damage states (*DSs*) based on the range of damage values (i.e., Minor damage, Moderate damage, Extensive damage). A Monte Carlo simulation (MCS) is used to model how the embankment settlement distributions change as the wetting front progresses.
3. The resultant probability of failure data is plotted with time to form the fragility curves. For each rainfall intensity and duration combination considered, three realisations of probability of exceedance and reliability index are determined.

The selection of appropriate damage states is crucial, and various *DSs* have been previously considered for road transport infrastructure. Criteria such as horizontal displacements at embankments and traffic lanes, maximum settlement of the embankment surface, lateral displacement rate, and maximum subsidence rate have been used to classify *DSs* in previous studies. Following Pitilakis et al. (2014) and Argyroudis and Kaynia (2015), this study adopts the mean settlement value (measured at the edge and middle of the embankment/cut surface) at the railroad embankment crest and delineates three *DSs* (minor, moderate, and extensive) to depict damage levels. Expert judgment-based descriptions of these damage levels are as follows: *DS*₁ indicates slight surface sliding or minor cracks on the road surface (corresponding to an embankment settlement of 0.03 m), with vehicle passage unaffected; *DS*₂ denotes the need for partial road closure due to medium settlement or cracks (corresponding to 0.08 m), signalling a maintenance state; and *DS*₃ signifies extensive cracks (corresponding to 0.20 m), requiring full road closure for reconstruction or partial closure during significant repairs (Pitilakis et al., 2014).

3 Results

In this study, rainfall (of a given intensity and duration) is taken as an intensity measure. Rainfall duration is depicted on the *x*-axis of the fragility curves (Xue and Gavin, 2008). Given that this study assumes a rainfall intensity of 10 mm/h as a baseline case, the total rainfall can be acquired by multiplying rainfall intensity and rainfall duration. The fragility curves for minor, moderate, and extensive damage states are developed. The coefficients of variation (COV) are assigned for probabilistic calculations. The geotechnical strength parameters and unit weight are defined using normal distributions as recommended by Phoon (2008), and Phoon and Kulhawy (1999). The mean values of embankment materials are summarised in Table 1. The COVs assigned to the unit weight, angle of internal friction, cohesion, and compression modulus are 0.1, 0.3, 0.5, and 0.5, respectively. A Monte Carlo probabilistic analysis was conducted. This section analyzes the fragility curve of the embankment considering the influence of the rainfall intensity, the fill saturated permeability and the embankment slope angles.

Figure 1 illustrates the fragility curves corresponding to rainfall intensities of 5, 10 and 18 mm/h, respectively. These curves indicate that within the initial 5 hours of rainfall, the likelihood of surpassing any damage state is nearly negligible. However, for longer rainfall durations, the probability of exceedance increases progressively, accompanied by extended time intervals between the damage states. When the duration

of rainfall is 8 h, all the probabilities of three rainfall intensities exceeding the limit state of the minor damage are approximately 0%. The embankment is unlikely to be affected by rainfall at this level. When the rainfall duration is 28 h, the probabilities of the rainfall intensities of 5, 10 and 18 mm/h exceeding the minor damage state are 6.4%, 18.1% and 96.9%. The studied embankment is likely to be slightly damaged at this rainfall duration. For very serious rainfall, for example, when the rainfall duration is 64 h, the extensive damage probability of the rainfall intensity of 18 mm/h reaches 27.2%. The embankment has a high fragility at extreme rainfall (e.g., rainfall durations longer than 96 h), and it may suffer instability.

Figure 2 illustrates the influence of embankment saturated permeability on the fragility curve, and the saturated permeability values of 0.77×10^{-6} m/s and 5.77×10^{-6} m/s are considered (Wu, 2011). The red curve represents the large permeability, while the black curve represents the low permeability. For the rainfall duration of 40 h, the probabilities of the saturated permeability values of 0.77×10^{-6} m/s and 5.77×10^{-6} m/s exceeding the minor damage state are 47.4% and 81.9%, respectively. At this rainfall duration, the embankment is prone to minor damage. In the case of a longer rainfall duration, such as 72 h, the probability of extensive damage for the saturated permeability of 5.77×10^{-6} m/s reaches 19.6%, indicating a high fragility to extreme rainfall events.

Figure 3 presents the influence of the embankment slope angle on the fragility curves. The slope angles corresponding to 2H: 1V and 1.5H: 1V are represented by the black and red lines, respectively. When the rainfall duration extends to 32 h, the probability of exceeding the minor damage state stands at 24.2% for slope angles of 2H: 1V and 37.1% for 1.5H: 1V. This indicates a propensity for minor damage in the studied embankment under such conditions. For a longer rainfall duration of 72 h, the probability of extensive damage for a slope angle of 1.5H: 1V is 20.4%. That emphasizes the increased susceptibility of the embankment to severe damage under extreme rainfall conditions.

4 Discussion

The influence of rainfall intensity, embankment saturated permeability, and slope angle varies in shaping the fragility curve. As shown in Figure 1, the fragility curves for the lower-intensity rainfall events shift towards higher probabilities, reflecting the extended development of the wetting front. Once the degradation process begins, the curves assume a consistent shape for different rainfall intensities. This is because the rainfall intensity has a negligible effect on the infiltration process post-wetting front development. However, the infiltration process post-wetting front development primarily hinges on the saturated permeability value and geometric parameters. As shown in Figure 2, the curve for the large permeability is steeper, indicating the embankment of saturated permeability values of 5.77×10^{-6} m/s is more sensitive to rainfall. A large permeability results in great wetting front progression and large probabilities of exceeding all three damage states, leading to steeper fragility curves. The results highlight the pivotal role of saturated permeability in shaping embankment fragility curves and consequently determining the risk associated with damage states. As the damage state transitions from minor to extensive, the difference in slope between the curves widens,

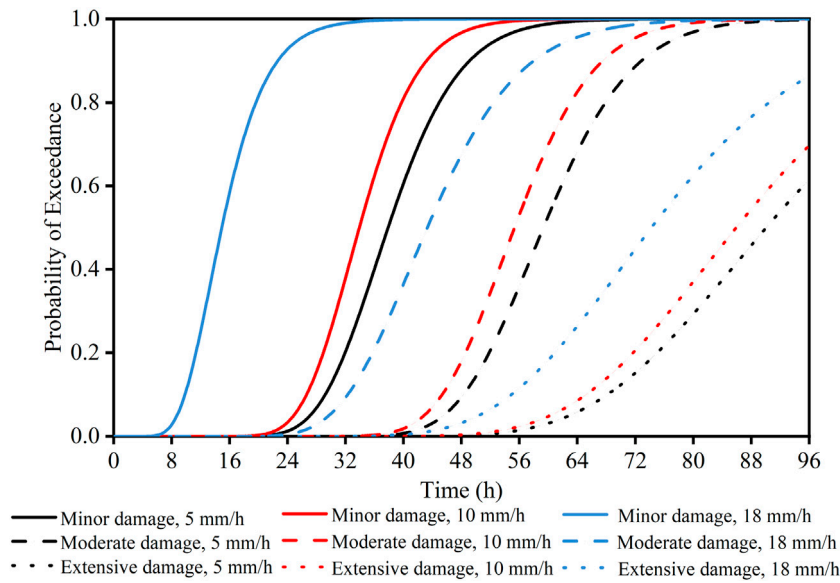


FIGURE 1
Fragility curves for rainfall intensities of 5, 10 and 18 mm/h.

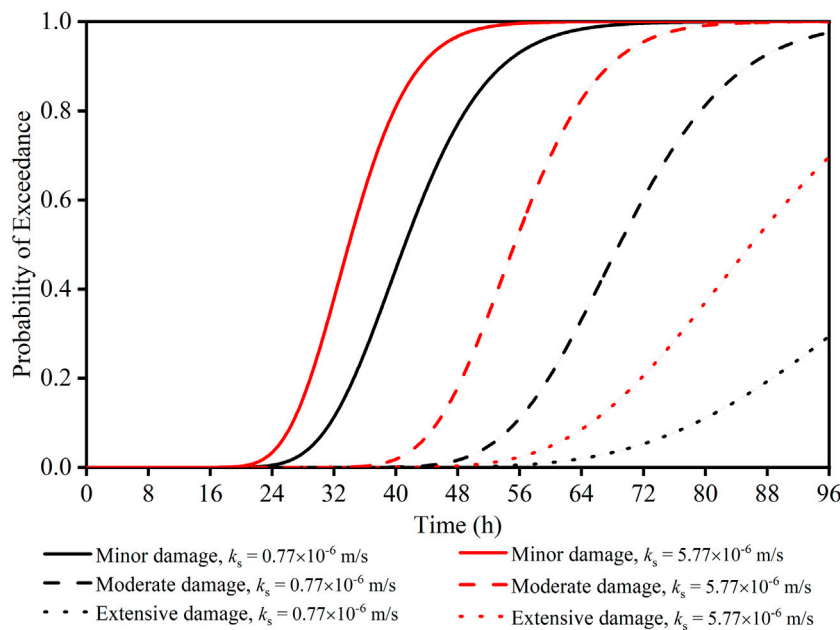


FIGURE 2
Fragility curves for saturated permeabilities of 0.77×10^{-6} m/s and 5.77×10^{-6} m/s.

emphasizing varying wetting front progression. Additionally, a high-angle embankment slope results in a steep fragility curve trend, as shown in Figure 3, suggesting increased susceptibility to settlement triggered by rainfall. A lower slope angle reduces the advancement of the wetting front, leading to decreased probabilities of exceeding all three damage states. Conversely, a higher slope angle accelerates downward seepage, resulting in more pronounced fragility curves. These findings emphasize the substantial impact

of the slope angles on embankment fragility curves and their implications for assessing risks associated with damage states.

5 Conclusion

This paper establishes rainfall-induced fragility curves for embankments on silty soils to improve the understanding of the

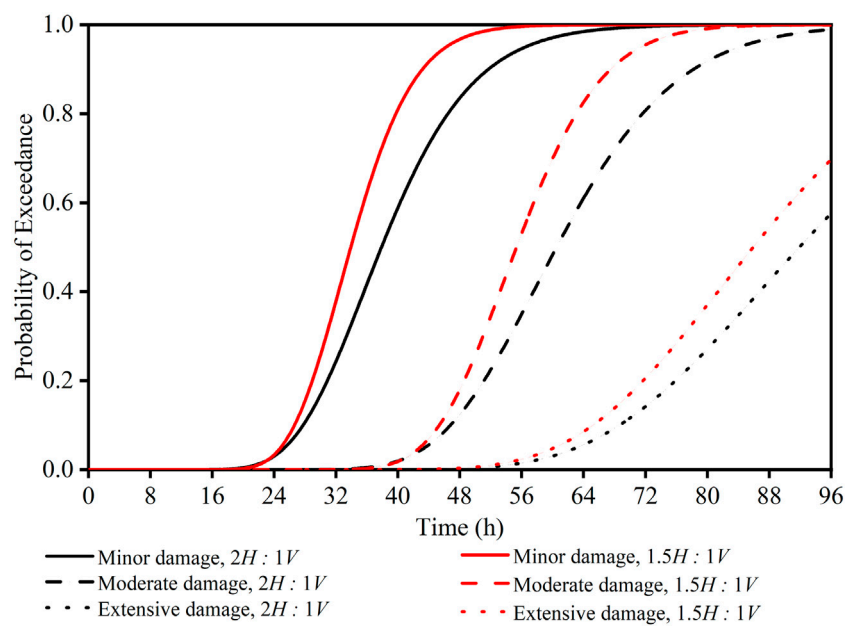


FIGURE 3
Fragility curves for slope angle of 2H: 1V and 1.5H: 1V.

rainfall-induced risk assessment of road embankment infrastructure. Nonlinear creep and deformation analyses using Monte Carlo simulations are carried out with reference to geometrical schemes and site conditions corresponding to the embankment in site from prior literature. The embankment performance is estimated using the *DS* in terms of the settlement of the embankment crest.

Fragility curves show that embankments subjected to higher rainfall intensity are more vulnerable to rainfall-induced deformation. That is captured by the increase in damage probability across all states with higher rainfall intensity. For extreme rainfall of 18 mm/h, when the rainfall duration is 64 h, the extensive damage probability reaches 27.2%. The fragility curves for high-intensity rainfall events indicate the accelerated progression of the wetting front. Once the degradation process begins, the curves show a consistent shape for different rainfall intensities.

The key role of saturated permeability and slope angle is highlighted in shaping embankment fragility curves and consequently determining the risk associated with various damage states. Higher saturated permeability and slope angle contribute to steeper fragility curves due to reduced soil suction and a lower wetting front. Fragility curves serve as valuable tools for transport network operators, enabling them to make informed decisions about service closures based on detailed weather forecasts and the assessment of damage risk exceeding permissible limits.

Note that the analyses that have been presented show that the shape of the fragility curve depends on environmental loading (rainfall intensity and duration), soil parameters and geometric parameters. The fragility is also influenced by the initial soil suction, soil-water characteristic curve (SWCC) and other parameters, which are expected to be considered in future work.

Data availability statement

The original contributions presented in the study are included in the article/supplementary material, further inquiries can be directed to the corresponding author.

Author contributions

HZ: Writing–review and editing, Supervision, Methodology, Conceptualization, Writing–original draft. FM: Writing–original draft, Software, Methodology, Data curation. XY: Writing–review and editing, Writing–original draft, Methodology, Formal Analysis, Conceptualization. GZ: Writing–review and editing, Methodology, Conceptualization.

Funding

The author(s) declare that financial support was received for the research, authorship, and/or publication of this article. The research reported in this paper was supported by the National Natural Science Foundation of China (No. 52322809, No. 52078337 and No. 52208363) and the Natural Science Foundation of Hebei, China (No. E2021202215).

Conflict of interest

The authors declare that the research was conducted in the absence of any commercial or financial relationships that could be construed as a potential conflict of interest.

Publisher's note

All claims expressed in this article are solely those of the authors and do not necessarily represent those of their affiliated

organizations, or those of the publisher, the editors and the reviewers. Any product that may be evaluated in this article, or claim that may be made by its manufacturer, is not guaranteed or endorsed by the publisher.

References

- Achillopoulou, D. V., Mitoulis, S. A., Argyroudis, S. A., and Wang, Y. (2020). Monitoring of transport infrastructure exposed to multiple hazards: a roadmap for building resilience. *Sci. total Environ.* 746, 141001. doi:10.1016/j.scitotenv.2020.141001
- Argyroudis, S., and Kaynia, A. M. (2015). Analytical seismic fragility functions for highway and railway embankments and cuts. *Earthq. Eng. Struct. Dyn.* 44 (11), 1863–1879. doi:10.1002/eqe.2563
- Argyroudis, S. A., Mitoulis, S. A., Winter, M. G., and Kaynia, A. M. (2019). Fragility of transport assets exposed to multiple hazards: state-of-the-art review toward infrastructural resilience. *Reliab. Eng. Syst. Saf.* 191, 106567. doi:10.1016/j.res.2019.106567
- Babu, G. S., and Murthy, D. S. (2005). Reliability analysis of unsaturated soil slopes. *J. geotechnical geoenvironmental Eng.* 131 (11), 1423–1428. doi:10.1061/(asce)1090-0241(2005)131:11(1423)
- Chen, K., Liang, F., and Wang, C. (2021). A fractal hydraulic model for water retention and hydraulic conductivity considering adsorption and capillarity. *J. Hydrology* 602, 126763. doi:10.1016/j.jhydrol.2021.126763
- Chen, K., Pang, R., and Xu, B. (2023). Stochastic dynamic response and seismic fragility analysis for high concrete face rockfill dams considering earthquake and parameter uncertainties. *Soil Dyn. Earthq. Eng.* 167, 107817. doi:10.1016/j.soildyn.2023.107817
- Chen, W. Z., Jiang, G. L., Zhao, H. S., Wu, L. J., and Li, A. H. (2014). Analysis of nonlinear settlement for an unsaturated soil under stage continuous loading. *J. Central South Univ.* 21, 4690–4697. doi:10.1007/s11771-014-2478-2
- Gavin, K., and Xue, J. (2009). Use of a genetic algorithm to perform reliability analysis of unsaturated soil slopes. *Géotechnique* 59 (6), 545–549. doi:10.1680/geot.8.t.004
- Huang, J., and Han, J. (2009). 3D coupled mechanical and hydraulic modeling of a geosynthetic-reinforced deep mixed column-supported embankment. *Geotext. Geomembranes* 27 (4), 272–280. doi:10.1016/j.geotextmem.2009.01.001
- Itasca Consulting Group (2017). *Flac 3D – fast Lagrangian analysis of continua in 3 dimensions, ver. 6.0*. Minneapolis, Minnesota: Itasca.
- Lu, Y., Pang, R., Du, M., and Xu, B. (2024). Simulation of non-stationary ground motions and its applications in high concrete faced rockfill dams via direct probability integral method. *Eng. Struct.* 298, 117034. doi:10.1016/j.engstruct.2023.117034
- Martinović, K., Reale, C., and Gavin, K. (2018). Fragility curves for rainfall-induced shallow landslides on transport networks. *Can. Geotechnical J.* 55 (6), 852–861. doi:10.1139/cgj-2016-0565
- K. K. Phoon (2008). *Reliability-based design in geotechnical engineering: computations and applications*. New York, NY, United States: (Taylor and Francis).
- Phoon, K. K., and Kulhawy, F. H. (1999). Characterization of geotechnical variability. *Can. Geotechnical J.* 36 (4), 612–624. doi:10.1139/cgj-36-4-612
- Pitilakis, K., Crowley, H., and Kaynia, A. M. (2014). SYNER-G: typology definition and fragility functions for physical elements at seismic risk. *Geotechnical, Geol. Earthq. Eng.* 27, 1–28. doi:10.1007/978-94-007-7872-6
- Reale, C., Xue, J., and Gavin, K. (2016b). System reliability of slopes using multimodal optimisation. *Géotechnique* 66 (5), 413–423. doi:10.1680/jgeot.15.p.142
- Reale, C., Xue, J. F., Pan, Z., and Gavin, K. (2015). Deterministic and probabilistic multimodal analysis of slope stability. *Comput. Geotechnics* 66 (5), 172–179. doi:10.1016/j.compgeo.2015.01.017
- Reeves, S., Winter, M., Leal, D., and Hewitt, A. (2019a). *Rail: an industry guide to enhancing resilience*. The Resilience Shift and TRL: London, UK.
- Reeves, S., Winter, M., Leal, M., and Hewitt, D. (2019b). *Roads: an industry guide to enhancing resilience*. London, UK: TRL and the Resilience Shift.
- Thorne, C. (2014). Geographies of UK flooding in 2013/4. *Geogr. J.* 180 (4), 297–309. doi:10.1111/geoj.12122
- Wang, C., Yuan, Y., Liang, F., and Tao, J. (2022). Experimental investigation of local scour around cylindrical pile foundations in a double-layered sediment under current flow. *Ocean. Eng.* 251, 111084. doi:10.1016/j.oceaneng.2022.111084
- Winter, M. G., Reeves, S. J., Smajlović, S., Ghataora, G., Šehić, D., and Zejnić, H. (2020). The Kosova landslide, Bosnia and Herzegovina. *Q. J. Eng. Geol. Hydrogeology* 53 (4), 523–529. doi:10.1144/qjegh2019-097
- Wu, L. J. (2011). *Study on compressibility and consolidation of unsaturated soil and reinforced technique on high-speed railway*. Chengdu, China: Southwest Jiaotong University.
- Xu, M., Pang, R., Zhou, Y., and Xu, B. (2023). Seepage safety evaluation of high earth-rockfill dams considering spatial variability of hydraulic parameters via subset simulation. *J. Hydrology* 626, 130261. doi:10.1016/j.jhydrol.2023.130261
- Xue, J., and Gavin, K. (2008). Effect of rainfall intensity on infiltration into partly saturated slopes. *Geotechnical Geol. Eng.* 26, 199–209. doi:10.1007/s10706-007-9157-0
- Xue, J. F., and Gavin, K. (2007). Simultaneous determination of critical slip surface and reliability index for slopes. *J. geotechnical geoenvironmental Eng.* 133 (7), 878–886. doi:10.1061/(asce)1090-0241(2007)133:7(878)
- Zheng, G., Guo, Z., Zhou, H., and He, X. (2024a). Design method for wall deformation and soil movement of excavations with inclined retaining walls in sand. *Int. J. Geomechanics* 24 (4), doi:10.1061/jgnai.gmeng-9029
- Zheng, G., Guo, Z., Zhou, H., Tan, Y., Wang, Z., and Li, S. (2024b). Multibenched excavations with inclined-vertical framed retaining walls in soft soils: observations and numerical investigation. *J. Geotechnical Geoenvironmental Eng.* 150 (5), doi:10.1061/jggefkgeng-11943
- Zheng, G., Yang, X., Zhou, H., and Chai, J. (2019). Numerical modeling of progressive failure of rigid piles under embankment load. *Can. Geotechnical J.* 56 (1), 23–34. doi:10.1139/cgj-2017-0613
- Zhou, H., Liu, X., Tan, J., Zhao, J., and Zheng, G. (2023). Seismic fragility evaluation of embankments on liquefiable soils and remedial countermeasures. *Soil Dyn. Earthq. Eng.* 164, 107631. doi:10.1016/j.soildyn.2022.107631
- Zhou, H., Zhang, J., Yu, X., Hu, Q., Zheng, G., Xu, H., et al. (2024). Stochastic bearing capacity and failure mechanism of footings placed adjacent to slopes considering the anisotropic spatial variability of the clay undrained strength. *Int. J. Geomechanics* 24 (4), doi:10.1061/jgnai.gmeng-9136